Available online at www.sciencedirect.com
SCIENCE DIRECT®
Journal of Sound and Vibration 282 (2005) 125–149
JOURNAL OF SOUND AND VIBRATION
www.elsevier.com/locate/jsvi

Responses of infinite periodic structures to moving or stationary harmonic loads

X. Sheng*, C.J.C. Jones, D.J. Thompson

University of Southampton, Highfield, Southampton SO17 1BJ, England, UK

Received 26 August 2003; accepted 16 February 2004
Available online 14 October 2004

Abstract

Formulae are derived for the computation of the response of periodically supported structures subject to a moving or stationary harmonic load. They are expressed in terms of an integral over the wavenumber in the longitudinal direction. The structures may be described using either a multiple-beam model, or more generally, a two-and-half-dimensional finite-element model. The supports, described by a receptance matrix, may have arbitrary degrees of freedom, either translational or rotational. Equations for free vibration propagation constants are yielded straightforwardly. Results are produced for a conventional ballasted track, showing the effects of the load speed and the modelling of the supports.

1. Introduction

Vibration of infinite periodic structures has been studied extensively in the past 30 years with the focus mainly on free vibration propagation and forced vibration induced by stationary harmonic loads [1]. The stationary forced vibration model has been heavily employed to model railway tracks in the study of rolling noise [2] and other wheel/rail interaction problems [3]. It is

*Corresponding author. Current address: Applied Mechanics Group, Tech Centre, Holset Engineering, St. Andrew's Road, Huddersfield HD1 6RA, UK.
E-mail address: shengxiaozhen@hotmail.com (X. Sheng).

0022-460X/$ - see front matter © 2004 Elsevier Ltd. All rights reserved.
doi:10.1016/j.jsv.2004.02.050

found that the direct receptances of the rail above a sleeper and at mid-span are greatly different at frequencies close to the so-called pinned–pinned frequency, which for modern ballasted tracks, is about 1000 Hz. The pinned–pinned frequency occurs due to the discrete supports provided to the rails by identically spaced sleepers. It is a resonance frequency at mid-span while above a sleeper it is an anti-resonance frequency. No pinned–pinned frequency exists if a 'continuous support model' is used. However, it is not clear what the effect is of the load speed on the pinned–pinned phenomena. It is also not clear if the load speed reduces or enhances the difference between the 'discrete support model' and the 'continuous support model'. To answer these questions, and for other applications such as rail roughness growth, the forced vibration of a track due to a moving excitation must be investigated.

Vibration of an infinite periodic beam subject to a moving harmonic load has been investigated in Ref. [4]. In this study, the author considered a single segment only by using boundary conditions derived according to the Euler beam theory. It must be acknowledged that the mathematical treatments used in this reference are very idea-inspirational. Nordborg [5] also used an Euler beam model to represent a moving load on a periodically supported rail. However, in the calculation of the varying stiffness of the track, the author sets $x = ct$ (where c is the speed of the moving wheel) in the receptance, $\alpha_p(x, \omega)$, of the rail at the loading point, x, due to a unit *stationary* harmonic load of frequency ω, and then inverses the receptance to give the time-dependent stiffness of the track. This means to give the varying track stiffness has also been used by other researchers. For high-frequency vibration of a periodic structure like a track, it may be inappropriate to model the structure as a single beam, especially for lateral vibration of the rail [6–8], and therefore the formulae derived in Refs. [4,5] are not applicable. An alternative must be developed.

In this paper a more general, wavenumber-based approach is proposed to study the response of an infinite periodic structure to moving and stationary harmonic loads. In this approach the periodically supported structure is represented as either a multiple-beam model, or more generally, a two-and-half-dimensional (2.5D) finite-element model [9,10]. The 2.5D FEM requires the structure to be homogeneous in the longitudinal direction but its cross-section can be arbitrarily shaped. Although the approach developed in this paper can be applied to any periodic structure subject to moving or stationary harmonic loads, it is intended here to identify the effects of the load speed on the dynamics of conventional railway tracks and on the difference between the 'discrete support model' and the 'continuous support model'.

2. Differential equation of a periodic structure

Suppose an elastic body is infinitely long in the longitudinal (x-) direction and its cross-sections normal to the x-axis are invariant with x. A unique discretization is made for every cross-section, and nodal lines parallel to the x-axis are formed by nodes in a cross-section and corresponding counterparts in other cross-sections. The displacements of the n nodes on the x cross-section are

denoted by a $3n$ vector

$$\{q(x,t)\} = (u_1, v_1, w_1, \ldots, u_n, v_n, w_n)^{\mathrm{T}} \tag{1}$$

where u, v, w are displacement components in the x-, y- and z-directions. According to the 2.5D FEM [9,10], the differential equation of motion of the structure is given by

$$[\mathbf{M}]\{\ddot{q}(x,t)\} + [\mathbf{K}]_0\{q(x,t)\} + [\mathbf{K}]_1\frac{\partial}{\partial x}\{q(x,t)\} - [\mathbf{K}]_2\frac{\partial^2}{\partial x^2}\{q(x,t)\} = \{F(x,t)\}, \tag{2}$$

where $\{F(x,t)\}$ denotes the nodal force vector, in units N/m. In Eq. (2), $[\mathbf{M}]$, $[\mathbf{K}]_0$ and $[\mathbf{K}]_2$ are $3n \times 3n$ symmetric matrices, and $[\mathbf{K}]_1$ is an anti-symmetric matrix. Further, $[\mathbf{M}]$ and both the real and imaginary parts of $[\mathbf{K}]_2$ are positive definite and both the real and imaginary parts of $[\mathbf{K}]_0$ are non-negative. As shown in Section 5, the dynamics of a single or a multiple Timoshenko beam model can also be described by Eq. (2), except that the degrees of freedom of each beam at x consist of a translation and rotation(s).

It is further assumed that at every length l in the x-direction, a support having arbitrary degrees of freedom is connected to the elastic body. All the supports are assumed to be identical, and therefore a periodic structure is formed. The supports may produce not only point forces to part of the nodes, but also torques in planes containing a nodal line. The point forces produced by the jth support at $x = jl$ are denoted by a force vector $\{F_j(t)\}$ containing N_p components and the torques by a torque vector $\{M_j(t)\}$ consisting N_t components. This torque vector may be represented by two force vectors, $\{M_j(t)\}/\Delta x$ and $-\{M_j(t)\}/\Delta x$, applied at two cross-sections separated by a distance Δx : $x = jl + \Delta x$ and $x = jl$ (note: the components corresponding to x must be zero). Thus the nodal force vector provided by the supports is given by

$$\{F_c(x,t)\} = \sum_{j=-\infty}^{\infty}\delta(x-jl)[\mathbf{T}]_p\{F_j(t)\} + \frac{1}{\Delta x}\sum_{j=-\infty}^{\infty}(\delta(x-jl-\Delta x)-\delta(x-jl))[\mathbf{T}]_t\{M_j(t)\}, \tag{3}$$

where $\delta(\cdot)$ is the delta-function, $[\mathbf{T}]_p$ is a matrix of order $3n \times N_p$, $N_p \leqslant 3n$, with elements being either unit or zero and such that $[\mathbf{T}]_p^{\mathrm{T}}[\mathbf{T}]_p$ is a unit matrix of $N_p \times N_p$. If the jth element of $\{F_j(t)\}$ acts at the ith degree of freedom of the elastic body, then $T_p(i,j) = 1$; otherwise $T_p(i,j) = 0$. $[\mathbf{T}]_t$ is similar to $[\mathbf{T}]_p$ but is of order $3n \times N_t$, where $N_t \leqslant 3n$. The connection between the elastic body and each of the supports requires that

$$[\mathbf{T}]_p^{\mathrm{T}}\{q(kl,t)\} \equiv -L_p(\{F_k(t)\},\{M_k(t)\}), \quad k = -\infty, \ldots, 0, \ldots, \infty, \tag{4a}$$

$$[\mathbf{T}]_t^{\mathrm{T}}\frac{\partial}{\partial x}\{q(kl,t)\} \equiv -L_t(\{F_k(t)\},\{M_k(t)\}), \quad k = -\infty, \ldots, 0, \ldots, \infty, \tag{4b}$$

where the operators L_p and L_t describe the dynamical responses of the support. The minus sign before the operators indicates that $\{F_k(t)\}$ is opposite in direction to the positive displacement of the support.

The externally applied loads are assumed to be harmonic with radian frequency Ω and moving in the x-direction at speed c. At $t = 0$, the loads are applied at the x_0 cross-section. The

corresponding nodal force vector is given by

$$\{F_e(x,t)\} = \delta(x - x_0 - ct)\{P_0\}e^{i\Omega t}, \tag{5}$$

where $\{P_0\} \in C^{3n}$ denotes the amplitude vector of the loads. The case of stationary excitation results if $c = 0$. Substitution of Eqs. (3) and (5) into Eq. (2) yields

$$[\mathbf{M}]\{\ddot{q}(x,t)\} + [\mathbf{K}]_0\{q(x,t)\} + [\mathbf{K}]_1\frac{\partial}{\partial x}\{q(x,t)\} - [\mathbf{K}]_2\frac{\partial^2}{\partial x^2}\{q(x,t)\} = \{F_e(x,t)\} + \{F_c(x,t)\}. \tag{6}$$

3. Solution for the periodic structure subject to moving harmonic loads

As shown in Eq. (6), the excitations consist of two parts. Therefore the nodal displacement vector $\{q(x,t)\}$ may also be divided into two parts, i.e.,

$$\{q(x,t)\} = \{q_e(x,t)\} + \{q_c(x,t)\}, \tag{7}$$

where $\{q_e(x,t)\}$ is due to the externally applied loads and satisfies

$$\begin{aligned}[\mathbf{M}]\{\ddot{q}_e(x,t)\} + [\mathbf{K}]_0\{q_e(x,t)\} + [\mathbf{K}]_1\frac{\partial}{\partial x}q_e(x,t)\} - [\mathbf{K}]_2\frac{\partial^2}{\partial x^2}\{q_e(x,t)\}\\ = \{F_e(x,t)\} = \delta(x - x_0 - ct)\{P_0\}e^{i\Omega t}\end{aligned} \tag{8}$$

and $\{q_c(x,t)\}$, generated by the supports, satisfies

$$\begin{aligned}[\mathbf{M}]\{\ddot{q}_c(x,t)\} + [\mathbf{K}]_0\{q_c(x,t)\} + [\mathbf{K}]_1\frac{\partial}{\partial x}\{q_c(x,t)\} - [\mathbf{K}]_2\frac{\partial^2}{\partial x^2}\{q_c(x,t)\} = \{F_c(x,t)\}\\ = \sum_{j=-\infty}^{\infty}\delta(x - jl)[\mathbf{T}]_p\{F_j(t)\} + \frac{1}{\Delta x}\sum_{j=-\infty}^{\infty}(\delta(x - jl - \Delta x) - \delta(x - jl))[\mathbf{T}]_t\{M_j(t)\}.\end{aligned} \tag{9}$$

3.1. Solution for $\{q_e(x,t)\}$

The solution of Eq. (8) for $\{q_e(x,t)\}$ is described in Ref. [9], and may be expressed as

$$\{q_e(x,t)\} = [\mathbf{Q}_e(x - x_0 - ct)]\{P_0\}e^{i\Omega t}, \tag{10}$$

where, by denoting

$$\omega = \Omega - \beta c, \tag{11}$$

$$[\mathbf{D}(\beta,\omega)] = -\omega^2[\mathbf{M}] + [\mathbf{K}]_0 + i\beta[\mathbf{K}]_1 + \beta^2[\mathbf{K}]_2, \tag{12}$$

$$[\tilde{\mathbf{Q}}_e(\beta)] = [\mathbf{D}(\beta,\omega)]^{-1}, \tag{13}$$

the $3n \times 3n$ matrix $[\mathbf{Q}_e(x)]$ is determined by performing an inverse Fourier transform for $[\tilde{\mathbf{Q}}_e(\beta)]$, i.e.,

$$[\mathbf{Q}_e(x)] = \frac{1}{2\pi}\int_{-\infty}^{\infty} [\tilde{\mathbf{Q}}_e(\beta)] \mathrm{e}^{\mathrm{i}\beta x}\,\mathrm{d}\beta, \tag{14}$$

where $\mathrm{i} = \sqrt{-1}$, β is the wavenumber in the x-direction in units rad/m. Eq. (10) shows that $\{q_e(x,t)\}$ is harmonic if $x' = x - x_0 - ct$ is fixed (i.e. observed from the moving loads) and the frequency is identical to that of the excitation. For stationary loads where $c = 0$, $[\mathbf{Q}_e(x)]$ can be expressed analytically in terms of the roots (for β) of $\det([\mathbf{D}(\beta,\omega)])$. It can be shown that the Fourier transform of Eq. (10) with respect to time t (that is the displacement spectrum) is given by

$$\{\hat{q}_e(x,f)\} = \int_{-\infty}^{\infty} \{q_e(x,t)\}\mathrm{e}^{-\mathrm{i}2\pi ft}\,\mathrm{d}t = \frac{1}{c}\mathrm{e}^{\mathrm{i}\beta^*(x-x_0)}[\tilde{\mathbf{Q}}_e(\beta^*)]\{P_0\}, \tag{15}$$

where

$$\beta^* = (\Omega - 2\pi f)/c,\ [\tilde{\mathbf{Q}}_e(\beta^*)] = [\mathbf{D}(\beta^*, 2\pi f)]^{-1}. \tag{16}$$

3.2. Solution for $\{q_c(x,t)\}$

To solve Eq. (9), the Fourier transform with respect to x (from x to wavenumber β) is performed

$$\begin{aligned}
&[\mathbf{M}]\{\ddot{\bar{q}}_c(\beta,t)\} + [\mathbf{K}]_0\{\bar{q}_c(\beta,t)\} + \mathrm{i}\beta[\mathbf{K}]_1\{\bar{q}_c(\beta,t)\} + \beta^2[\mathbf{K}]_2\{\bar{q}_c(\beta,t)\}\\
&\quad = \sum_{j=-\infty}^{\infty}[\mathbf{T}]_p\{F_j(t)\}\mathrm{e}^{-\mathrm{i}\beta jl} + \sum_{j=-\infty}^{\infty}[\mathbf{T}]_t\{M_j(t)\}\frac{1}{\Delta x}(\mathrm{e}^{-\mathrm{i}\beta(jl+\Delta x)} - \mathrm{e}^{-\mathrm{i}\beta jl})\\
&\quad = \sum_{j=-\infty}^{\infty}[\mathbf{T}]_p\{F_j(t)\}\mathrm{e}^{-\mathrm{i}\beta jl} + \sum_{j=-\infty}^{\infty}[\mathbf{T}]_t\{M_j(t)\}\frac{\partial}{\partial x}\mathrm{e}^{-\mathrm{i}\beta x}\Big|_{x=jl}\\
&\quad = \sum_{j=-\infty}^{\infty}[\mathbf{T}]_p\{F_j(t)\}\mathrm{e}^{-\mathrm{i}\beta jl} - \mathrm{i}\beta\sum_{j=-\infty}^{\infty}[\mathbf{T}]_t\{M_j(t)\}\mathrm{e}^{-\mathrm{i}\beta jl}.
\end{aligned} \tag{17}$$

For this equation, the Fourier transform is further performed but with respect to time t:

$$\begin{aligned}
&(-(2\pi f)^2[\mathbf{M}] + [\mathbf{K}]_0 + \mathrm{i}\beta[\mathbf{K}]_1 + \beta^2[\mathbf{K}]_2)\{\hat{\bar{q}}_c(\beta,f)\}\\
&\quad = \sum_{j=-\infty}^{\infty}[\mathbf{T}]_p\{\hat{F}_j(f)\}\mathrm{e}^{-\mathrm{i}\beta jl} - \mathrm{i}\beta\sum_{j=-\infty}^{\infty}[\mathbf{T}]_t\{\hat{M}_j(f)\}\mathrm{e}^{-\mathrm{i}\beta jl},
\end{aligned} \tag{18}$$

where

$$\{\hat{F}_j(f)\} = \int_{-\infty}^{\infty}\{F_j(t)\}\mathrm{e}^{-\mathrm{i}2\pi ft}\,\mathrm{d}t,\ \{\hat{M}_j(f)\} = \int_{-\infty}^{\infty}\{M_j(t)\}\mathrm{e}^{-\mathrm{i}2\pi ft}\,\mathrm{d}t.$$

From Eq. (18)

$$\{\hat{\bar{q}}_c(\beta,f)\} = [\mathbf{D}(\beta,2\pi f)]^{-1}\sum_{j=-\infty}^{\infty}([\mathbf{T}]_p\{\hat{F}_j(f)\} - \mathrm{i}\beta[\mathbf{T}]_t\{\hat{M}_j(f)\})\mathrm{e}^{-\mathrm{i}\beta jl}, \tag{19}$$

where matrix $[\mathbf{D}]$ is defined by Eq. (12).

Due to the regular repetition of the supports connected to the elastic body and the nature of the excitation, the constraint force and torque vectors are identical apart from a time lag,

$$\left\{F_j\left(t+\frac{jl}{c}\right)\right\} = \{F_0(t)\}\mathrm{e}^{\mathrm{i}\Omega jl/c}, \quad j=-\infty,\ldots,0,\ldots,\infty, \tag{20a}$$

$$\left\{M_j\left(t+\frac{jl}{c}\right)\right\} = \{M_0(t)\}\mathrm{e}^{\mathrm{i}\Omega jl/c}, \quad j=-\infty,\ldots,0,\ldots,\infty, \tag{20b}$$

where $\{F_0(t)\}$ and $\{M_0(t)\}$ are the supporting force and torque vectors at the 0th support where $x=0$. Thus the Fourier transforms of them with respect to t are given by

$$\{\hat{F}_j(f)\} = \{\hat{F}_0(f)\}\mathrm{e}^{\mathrm{i}(\Omega-2\pi f)jl/c} = \{\hat{F}_0(f)\}\mathrm{e}^{\mathrm{i}\beta^* jl}, \tag{21a}$$

$$\{\hat{M}_j(f)\} = \{\hat{M}_0(f)\}\mathrm{e}^{\mathrm{i}(\Omega-2\pi f)jl/c} = \{\hat{M}_0(f)\}\mathrm{e}^{\mathrm{i}\beta^* jl}. \tag{21b}$$

Inserting Eqs. (21a) and (21b) into Eq. (19), gives

$$\{\hat{\tilde{q}}_c(\beta,f)\} = [\mathbf{D}(\beta,2\pi f)]^{-1}([\mathbf{T}]_p\{\hat{F}_0(f)\} - \mathrm{i}\beta[\mathbf{T}]_t\{\hat{M}_0(f)\})\sum_{j=-\infty}^{\infty}\mathrm{e}^{-\mathrm{i}(\beta-\beta^*)jl}, \tag{22}$$

It can be shown that

$$\sum_{j=-\infty}^{\infty}\mathrm{e}^{-\mathrm{i}(\beta-\beta^*)jl} = 2\pi\sum_{j=-\infty}^{\infty}\delta((\beta^*-\beta)l-2\pi j). \tag{23}$$

Thus

$$\{\hat{\tilde{q}}_c(\beta,f)\} = 2\pi[\mathbf{D}(\beta,2\pi f)]^{-1}([\mathbf{T}]_p\{\hat{F}_0(f)\} - \mathrm{i}\beta[\mathbf{T}]_t\{\hat{M}_0(f)\})\sum_{j=-\infty}^{\infty}\delta((\beta^*-\beta)l-2\pi j). \tag{24}$$

The inverse Fourier transform of Eq. (24) with respect to β therefore is given by

$$\begin{aligned}\{\hat{q}_c(x,f)\} &= \frac{1}{2\pi}\int_{-\infty}^{\infty}\{\hat{\tilde{q}}_c(\beta,f)\}\mathrm{e}^{\mathrm{i}\beta x}\,\mathrm{d}\beta \\ &= \frac{1}{l}\sum_{j=-\infty}^{\infty}[\mathbf{D}(\beta_j,2\pi f)]^{-1}([\mathbf{T}]_p\{\hat{F}_0(f)\} - \mathrm{i}\beta_j[\mathbf{T}]_t\{\hat{M}_0(f)\})\mathrm{e}^{\mathrm{i}\beta_j x},\end{aligned} \tag{25}$$

where

$$\beta_j = \beta^* - \frac{2\pi j}{l} = \frac{\Omega-2\pi f}{c} - \frac{2\pi j}{l} \tag{26}$$

Now from Eq. (4) it follows that

$$[\mathbf{T}]_p^{\mathrm{T}}\{\hat{q}_c(kl,f)\} = -[\mathbf{T}]_p^{\mathrm{T}}\{\hat{q}_e(kl,f)\} - [\mathbf{H}(f)]_{11}\{\hat{F}_k(f)\} - [\mathbf{H}(f)]_{12}\{\hat{M}_k(f)\},$$

$$[\mathbf{T}]_t^{\mathrm{T}}\frac{\partial}{\partial x}\{\hat{q}_c(kl,f)\} = -[\mathbf{T}]_t^{\mathrm{T}}\frac{\partial}{\partial x}\{\hat{q}_e(kl,f)\} - [\mathbf{H}(f)]_{21}\{\hat{F}_k(f)\} - [\mathbf{H}(f)]_{22}\{\hat{M}_k(f)\}$$

and according to Eq. (21a), (21b),

$$[\mathbf{T}]_p^{\mathrm{T}}\{\hat{q}_c(kl,f)\} = -[\mathbf{T}]_p^{\mathrm{T}}\{\hat{q}_e(kl,f)\} - [\mathbf{H}(f)]_{11}\{\hat{F}_0(f)\}\mathrm{e}^{\mathrm{i}\beta^* kl} - [\mathbf{H}(f)]_{12}\{\hat{M}_0(f)\}\mathrm{e}^{\mathrm{i}\beta^* kl}, \tag{27a}$$

$$[\mathbf{T}]_t^{\mathrm{T}}\frac{\partial}{\partial x}\{\hat{q}_c(kl,f)\} = -[\mathbf{T}]_t^{\mathrm{T}}\frac{\partial}{\partial x}\{\hat{q}_e(kl,f)\} - [\mathbf{H}(f)]_{21}\{\hat{F}_0(f)\}\mathrm{e}^{\mathrm{i}\beta^* kl} - [\mathbf{H}(f)]_{22}\{\hat{M}_0(f)\}\mathrm{e}^{\mathrm{i}\beta^* kl}, \tag{27b}$$

where

$$[\mathbf{H}(f)] = \begin{bmatrix} [\mathbf{H}(f)]_{11} & [\mathbf{H}(f)]_{12} \\ [\mathbf{H}(f)]_{21} & [\mathbf{H}(f)]_{22} \end{bmatrix} \tag{28}$$

is the receptance matrix of order $(N_p + N_t) \times (N_p + N_t)$ of the supports found by Fourier transforming the operators in Eq. (4). $[\mathbf{H}(f)] = 0$ if the supports are rigid. Eq. (27), combined with Eqs. (15) and (25), gives

$$\begin{aligned} &\frac{1}{l}\sum_{j=-\infty}^{\infty}[\mathbf{T}]_p^{\mathrm{T}}[\mathbf{D}(\beta_j, 2\pi f)]^{-1}[\mathbf{T}]_p\mathrm{e}^{\mathrm{i}\beta_j kl}\{\hat{F}_0(f)\} \\ &\quad -\frac{1}{l}\sum_{j=-\infty}^{\infty}(\mathrm{i}\beta_j)[\mathbf{T}]_p^{\mathrm{T}}[\mathbf{D}(\beta_j, 2\pi f)]^{-1}[\mathbf{T}]_t\mathrm{e}^{\mathrm{i}\beta_j kl}\{\hat{M}_0(f)\} \\ &\quad +[\mathbf{H}(f)]_{11}\{\hat{F}_0(f)\}\mathrm{e}^{\mathrm{i}\beta^* kl} + [\mathbf{H}(f)]_{12}\{\hat{M}_0(f)\}\mathrm{e}^{\mathrm{i}\beta^* kl} \\ &= -\frac{1}{c}\mathrm{e}^{\mathrm{i}\beta^*(kl-x_0)}[\mathbf{T}]_p^{\mathrm{T}}[\tilde{\mathbf{Q}}_e(\beta^*)]\{P_0\}, \end{aligned} \tag{29a}$$

$$\begin{aligned} &\frac{1}{l}\sum_{j=-\infty}^{\infty}(\mathrm{i}\beta_j)[\mathbf{T}]_t^{\mathrm{T}}[\mathbf{D}(\beta_j, 2\pi f)]^{-1}[\mathbf{T}]_p\mathrm{e}^{\mathrm{i}\beta_j kl}\{\hat{F}_0(f)\} \\ &\quad -\frac{1}{l}\sum_{j=-\infty}^{\infty}(\mathrm{i}\beta_j)^2[\mathbf{T}]_t^{\mathrm{T}}[\mathbf{D}(\beta_j, 2\pi f)]^{-1}[\mathbf{T}]_t\mathrm{e}^{\mathrm{i}\beta_j kl}\{\hat{M}_0(f)\} \\ &\quad +[\mathbf{H}(f)]_{21}\{\hat{F}_0(f)\}\mathrm{e}^{\mathrm{i}\beta^* kl} + [\mathbf{H}(f)]_{22}\{\hat{M}_0(f)\}\mathrm{e}^{\mathrm{i}\beta^* kl} \\ &= -\frac{\mathrm{i}\beta^*}{c}\mathrm{e}^{\mathrm{i}\beta^*(kl-x_0)}[\mathbf{T}]_t^{\mathrm{T}}[\tilde{\mathbf{Q}}_e(\beta^*)]\{P_0\}. \end{aligned} \tag{29b}$$

Since $\mathrm{e}^{\mathrm{i}\beta_j kl} = \mathrm{e}^{\mathrm{i}(\beta^* - 2\pi j/l)kl} = \mathrm{e}^{\mathrm{i}\beta^* kl}$, Eq. (29) is equivalent to

$$[\mathbf{A}(f)]\begin{Bmatrix} \{\hat{F}_0(f)\} \\ \{\hat{M}_0(f)\} \end{Bmatrix} = -\frac{1}{c}\mathrm{e}^{-\mathrm{i}\beta^* x_0}[\mathbf{B}(\beta^*)][\tilde{\mathbf{Q}}_e(\beta^*)]\{P_0\}, \tag{30}$$

where

$$[\mathbf{A}(f)] = \begin{bmatrix} [\mathbf{A}(f)]_{11} & [\mathbf{A}(f)]_{12} \\ [\mathbf{A}(f)]_{21} & [\mathbf{A}(f)]_{22} \end{bmatrix}, \tag{31a}$$

$$[\mathbf{A}(f)]_{11} = [\mathbf{T}]_p^{\mathrm{T}} \left(\frac{1}{l} \sum_{j=-\infty}^{\infty} [\mathbf{D}(\beta_j, 2\pi f)]^{-1} \right) [\mathbf{T}]_p + [\mathbf{H}(f)]_{11}, \tag{31b}$$

$$[\mathbf{A}(f)]_{12} = -[\mathbf{T}]_p^{\mathrm{T}} \left(\frac{1}{l} \sum_{j=-\infty}^{\infty} (\mathrm{i}\beta_j)[\mathbf{D}(\beta_j, 2\pi f)]^{-1} \right) [\mathbf{T}]_t + [\mathbf{H}(f)]_{12}, \tag{31c}$$

$$[\mathbf{A}(f)]_{21} = [\mathbf{T}]_t^{\mathrm{T}} \left(\frac{1}{l} \sum_{j=-\infty}^{\infty} (\mathrm{i}\beta_j)[\mathbf{D}(\beta_j, 2\pi f)]^{-1} \right) [\mathbf{T}]_p + [\mathbf{H}(f)]_{21}, \tag{31d}$$

$$[\mathbf{A}(f)]_{22} = -[\mathbf{T}]_t^{\mathrm{T}} \left(\frac{1}{l} \sum_{j=-\infty}^{\infty} (\mathrm{i}\beta_j)^2[\mathbf{D}(\beta_j, 2\pi f)]^{-1} \right) [\mathbf{T}]_t + [\mathbf{H}(f)]_{22}, \tag{31e}$$

$$[\mathbf{B}(\beta^*)] = \begin{bmatrix} [\mathbf{T}]_p^{\mathrm{T}} \\ \mathrm{i}\beta^*[\mathbf{T}]_t^{\mathrm{T}} \end{bmatrix}. \tag{32}$$

Thus $\{\hat{F}_0(f)\}$ and $\{\hat{M}_0(f)\}$ can be determined as

$$\begin{Bmatrix} \{\hat{F}_0(f)\} \\ \{\hat{M}_0(f)\} \end{Bmatrix} = -\frac{1}{c} \mathrm{e}^{-\mathrm{i}\beta^* x_0} [\mathbf{A}(f)]^{-1} [\mathbf{B}(\beta^*)][\tilde{\mathbf{Q}}_e(\beta^*)]\{P_0\}. \tag{33}$$

Inserting Eq. (16) into Eq. (33) yields the spectrum of the supporting force and torque vector at the 0th support

$$\begin{Bmatrix} \{\hat{F}_0(f)\} \\ \{\hat{M}_0(f)\} \end{Bmatrix} = -\frac{1}{c} \mathrm{e}^{-\mathrm{i}\beta^* x_0} [\mathbf{A}(f)]^{-1} [\mathbf{B}(\beta^*)][\mathbf{D}(\beta^*, 2\pi f)]^{-1}\{P_0\} \tag{34}$$

in which the spectral frequency f and wavenumber β^* are related through Eq. (16).

The displacement vector $\{q_c(x,t)\}$ is determined by performing an inverse Fourier transform of Eq. (25). That is

$$\begin{aligned}\{q_c(x,t)\} &= \int_{-\infty}^{\infty} \{\hat{q}_c(x,f)\} e^{i2\pi ft}\, df \\ &= \frac{1}{l}\sum_{j=-\infty}^{\infty} \int_{-\infty}^{\infty} [\mathbf{D}(\beta_j, 2\pi f)]^{-1} [[\mathbf{T}]_p - i\beta_j [\mathbf{T}]_t] \begin{Bmatrix} \{\hat{F}_0(f)\} \\ \{\hat{M}_0(f)\} \end{Bmatrix} e^{i\beta_j x} e^{i2\pi ft}\, df \\ &= \frac{1}{l}\sum_{j=-\infty}^{\infty} \int_{-\infty}^{\infty} [\mathbf{D}(\beta_j, 2\pi f)]^{-1} [\mathbf{B}(\beta_j)]^{\mathrm{T}} \begin{Bmatrix} \{\hat{F}_0(f)\} \\ \{\hat{M}_0(f)\} \end{Bmatrix} e^{i\beta_j x} e^{i2\pi ft}\, df. \end{aligned} \tag{35}$$

From Eq. (35) it can be seen that

$$\{q_c(x+l, t+l/c)\} = \{q_c(x,t)\} e^{i\Omega l/c} \tag{36}$$

Eq. (10) also indicates that $\{q_e(x+l, t+l/c)\} = \{q_e(x,t)\} e^{i\Omega l/c}$. In other words, the displacement of the periodic structure due to the defined excitation satisfies

$$\{q(x+l, t+l/c)\} = \{q(x,t)\} e^{i\Omega l/c}. \tag{37}$$

3.3. Solution expressed in terms of wavenumber

The solutions derived above (Eq. (35)) are expressed in terms of an infinite integral with respect to the spectral frequency f. It may be more convenient to express them in terms of the wavenumber β in the x-direction. This is because even at a very high frequency, the propagating wavenumber in a railway track is small in magnitude (e.g. from Ref. [10], for a standard UIC 60 rail it is less than 25 rad/m at 5000 Hz). This treatment is especially necessary for stationary loads with $c = 0$, since it makes c disappear from the denominator in the formulae. The transform from spectral frequency f to wavenumber β is realised though Eq. (16) (note: β^* has been replaced by β):

$$2\pi f = \Omega - \beta c = \omega, \quad df = -\frac{c}{2\pi}\, d\beta; \tag{38}$$

then Eqs. (31) and (32) become

$$[\mathbf{A}(\beta)] = \begin{bmatrix} [\mathbf{A}(\beta)]_{11} & [\mathbf{A}(\beta)]_{12} \\ [\mathbf{A}(\beta)]_{21} & [\mathbf{A}(\beta)]_{22} \end{bmatrix}, \tag{39a}$$

$$[\mathbf{A}(\beta)]_{11} = [\mathbf{T}]_p^{\mathrm{T}} \left(\frac{1}{l} \sum_{j=-\infty}^{\infty} [\mathbf{D}(\beta_j, \omega)]^{-1} \right) [\mathbf{T}]_p + [\mathbf{H}(\omega)]_{11}, \tag{39b}$$

$$[\mathbf{A}(\beta)]_{12} = -[\mathbf{T}]_p^{\mathrm{T}} \left(\frac{1}{l} \sum_{j=-\infty}^{\infty} (i\beta_j) [\mathbf{D}(\beta_j, \omega)]^{-1} \right) [\mathbf{T}]_t + [\mathbf{H}(\omega)]_{12}, \tag{39c}$$

$$[\mathbf{A}(\beta)]_{21} = [\mathbf{T}]_t^{\mathrm{T}} \left(\frac{1}{l} \sum_{j=-\infty}^{\infty} (i\beta_j) [\mathbf{D}(\beta_j, \omega)]^{-1} \right) [\mathbf{T}]_p + [\mathbf{H}(\omega)]_{21}, \tag{39d}$$

$$[\mathbf{A}(\beta)]_{22} = -[\mathbf{T}]_t^{\mathrm{T}}\left(\frac{1}{l}\sum_{j=-\infty}^{\infty}(\mathrm{i}\beta_j)^2[\mathbf{D}(\beta_j,\omega)]^{-1}\right)[\mathbf{T}]_t + [\mathbf{H}(\omega)]_{22}, \tag{39e}$$

$$[\mathbf{B}(\beta)] = \begin{bmatrix} [\mathbf{T}]_p^{\mathrm{T}} \\ \mathrm{i}\beta[\mathbf{T}]_t^{\mathrm{T}} \end{bmatrix}, \tag{40}$$

where according to Eq. (26), $\beta_j = \beta - 2\pi j/l$. From Eqs. (34) and (35)

$$\begin{Bmatrix} \{F_0(t)\} \\ \{M_0(t)\} \end{Bmatrix} = -\frac{1}{2\pi}\left(\int_{-\infty}^{\infty}\mathrm{e}^{-\mathrm{i}\beta x_0}[\mathbf{A}(\beta)]^{-1}[\mathbf{B}(\beta)][\mathbf{D}(\beta,\omega)]^{-1}\mathrm{e}^{-\mathrm{i}\beta ct}\,\mathrm{d}\beta\right)\{P_0\}\mathrm{e}^{\mathrm{i}\Omega t}, \tag{41}$$

$$\begin{aligned}\{q(x,t)\} &= \{q_e(x,t)\} + \{q_c(x,t)\} \\ &= [\mathbf{Q}_e(x - x_0 - ct)]\{P_0\}\mathrm{e}^{\mathrm{i}\Omega t} \\ &\quad + \left[\sum_{j=-\infty}^{\infty}\left(-\frac{1}{2\pi l}\mathrm{e}^{-\mathrm{i}2\pi jx/l}\int_{-\infty}^{\infty}[\mathbf{D}(\beta_j,\omega)]^{-1}[\mathbf{B}(\beta_j)]^{\mathrm{T}}[\mathbf{A}(\beta)]^{-1}[\mathbf{B}(\beta)][\mathbf{D}(\beta,\omega)]^{-1}\mathrm{e}^{\mathrm{i}\beta(x-x_0-ct)}\,\mathrm{d}\beta\right)\right] \\ &\quad \times\{P_0\}\mathrm{e}^{\mathrm{i}\Omega t},\end{aligned} \tag{42}$$

where $[\mathbf{Q}_e(x)]$ is given by Eq. (14).

3.4. Displacements observed from the moving loads

If observation is made from a reference frame moving together with the loads, then the displacements of the structure are given by Eq. (42) by setting $x = x' + x_0 + ct$, i.e.,

$$\begin{aligned}\{q(x',t)\} &= [\mathbf{Q}_e(x')]\{P_0\}\mathrm{e}^{\mathrm{i}\Omega t} \\ &\quad + \left[\sum_{j=-\infty}^{\infty}\left(-\frac{1}{2\pi l}\mathrm{e}^{-\mathrm{i}2\pi j(x'+x_0)/l}\int_{-\infty}^{\infty}[\mathbf{D}(\beta_j,\omega)]^{-1}[\mathbf{B}(\beta_j)]^{\mathrm{T}}[\mathbf{A}(\beta)]^{-1}[\mathbf{B}(\beta)][\mathbf{D}(\beta,\omega)]^{-1}\mathrm{e}^{\mathrm{i}\beta x'}\,\mathrm{d}\beta\right)\mathrm{e}^{-\mathrm{i}2\pi jct/l}\right] \\ &\quad \times\{P_0\}\mathrm{e}^{\mathrm{i}\Omega t},\end{aligned}$$

i.e.,

$$\{q(x',t)\} = \left([\mathbf{Q}_e(x')] + \sum_{j=-\infty}^{\infty}[\boldsymbol{\alpha}(x')]_j\mathrm{e}^{-\mathrm{i}2\pi j(x'+x_0+ct)/l}\right)\{P_0\}\mathrm{e}^{\mathrm{i}\Omega t}, \tag{43}$$

where

$$[\boldsymbol{\alpha}(x')]_j = -\frac{1}{2\pi l}\int_{-\infty}^{\infty}[\mathbf{D}(\beta_j,\omega)]^{-1}[\mathbf{B}(\beta_j)]^{\mathrm{T}}[\mathbf{A}(\beta)]^{-1}[\mathbf{B}(\beta)][\mathbf{D}(\beta,\omega)]^{-1}\mathrm{e}^{\mathrm{i}\beta x'}\,\mathrm{d}\beta. \tag{44}$$

It can be seen from Eq. (43) that the term in the bracket (termed *the amplitude* which is the displacement divided by the load) is a periodic function of time t with period equal to l/c. The average of the amplitude over a period is given by $[\mathbf{Q}_e(x')] + [\boldsymbol{\alpha}(x')]_0$. Therefore, the displacements

are not purely harmonic. This feature may cause difficulties in dealing with wheel/track interaction problems in the frequency domain, where harmonic responses are assumed for the wheel and rail at the contact points for harmonic inputs. It can also be seen that at $x_0 = 0$, the variation of the displacement amplitudes with time t varying over $[0, l/c]$ is equivalent to the variation due to the initial loading position, x_0, varying over $[0, l]$ at $t = 0$.

3.5. Responses of the elastic body under equivalent continuous support

An equivalent continuously supported system is formed by evenly distributing the receptance of the supports along each bay. This gives the receptance per unit length in the x-direction (actually the displacement due to a unit force per unit length): $l[\mathbf{H}(\omega)]$. The responses of such a structure are obtained by considering the $j = 0$ term only in Eqs. (39), (40) and (42). Thus,

$$[\mathbf{A}(\beta)]_{11} = [\mathbf{T}]_p^{\mathrm{T}}[\mathbf{D}(\beta,\omega)]^{-1}[\mathbf{T}]_p + l[\mathbf{H}(\omega)]_{11}, \tag{45a}$$

$$[\mathbf{A}(\beta)]_{12} = -\mathrm{i}\beta[\mathbf{T}]_p^{\mathrm{T}}[\mathbf{D}(\beta,\omega)]^{-1}[\mathbf{T}]_t + l[\mathbf{H}(\omega)]_{12}, \tag{45b}$$

$$[\mathbf{A}(\beta)]_{21} = \mathrm{i}\beta[\mathbf{T}]_t^{\mathrm{T}}[\mathbf{D}(\beta,\omega)]^{-1}[\mathbf{T}]_p + l[\mathbf{H}(\omega)]_{21}, \tag{45c}$$

$$[\mathbf{A}(\beta)]_{22} = \beta^2[\mathbf{T}]_t^{\mathrm{T}}[\mathbf{D}(\beta,\omega)]^{-1}[\mathbf{T}]_t + l[\mathbf{H}(\omega)]_{22}, \tag{45d}$$

$$\{q(x,t)\} = [\mathbf{Q}_e(x - x_0 - ct)]\{P_0\}\mathrm{e}^{\mathrm{i}\Omega t} - \frac{1}{2\pi}\left(\int_{-\infty}^{\infty}[\mathbf{D}(\beta,\omega)]^{-1}[\mathbf{B}(\beta)]^{\mathrm{T}}[\mathbf{A}(\beta)]^{-1}[\mathbf{B}(\beta)][\mathbf{D}(\beta,\omega)]^{-1}\mathrm{e}^{\mathrm{i}\beta(x-x_0-ct)}\,\mathrm{d}\beta\right)\{P_0\}\mathrm{e}^{\mathrm{i}\Omega t}. \tag{46}$$

Eq. (46) shows that, observed from the moving loads, the displacement is purely time-harmonic everywhere. It should be noted that, the displacement amplitude from the continuous support model is not equal to the average of the time-varying amplitude from the discrete support model, although they may be close to each other in many cases.

4. Free vibration propagation

The formulae derived in Section 3.3 are applicable to the case of a stationary harmonic load without any difficulty. It is shown by Eqs. (41) and (42) that the supporting forces/torques and displacements of the elastic body are purely time-harmonic. It can be seen that matrix $[\mathbf{A}(\beta)]$ in Eq. (39) is a periodic function of β with period equal to $2\pi/l$.

It is important to investigate the free vibration property of periodic structures. The free vibration property is described by a propagation constant, ε, such that $\{q(x+l,t)\} = \{q(x,t)\}\mathrm{e}^{\mathrm{i}\varepsilon}$ [1]. Eq. (30) indicates that, for free vibration to exist $[\mathbf{A}(\beta,\omega)]$ must be a singular matrix, i.e.,

$$\det([\mathbf{A}(\beta,\omega)] = 0, \tag{47}$$

where, since ω is independent of β (see Eq. (38)), matrix $[\mathbf{A}(\beta)]$ in Eq. (39) has been denoted alternatively by $[\mathbf{A}(\beta,\omega)]$. For a root of Eq. (47), $\bar{\beta}$ at given frequency ω, the free vibration of the

periodic structure takes the form of (see Eq. (42))

$$\{q(x,t)\} = \{q_c(x,t)\} = \left(\sum_{j=-\infty}^{\infty} [\mathbf{D}(\beta_j,\omega)]^{-1}[\mathbf{B}(\beta_j)]^{\mathrm{T}} \mathrm{e}^{\mathrm{i}(\bar{\beta}-2\pi j/l)x}\right)\{\phi\}\mathrm{e}^{\mathrm{i}\omega t}, \tag{48}$$

where $\beta_j = \bar{\beta} - 2\pi j/l$, $\{\phi\}$ is the eigenvector of matrix $[\mathbf{A}(\beta,\omega)]$ corresponding to $\bar{\beta}$. Eq. (48) shows that the free vibration is not a purely spatially harmonic wave, but it does indicate that $\{q(x+l,t)\} = \{q(x,t)\}\mathrm{e}^{\mathrm{i}\bar{\beta}l}$, therefore the propagation constant is given by

$$\varepsilon = \bar{\beta}l. \tag{49}$$

Since $[\mathbf{A}(\beta,\omega)]$ is a periodic function of β with period equal to $2\pi/l$, $\bar{\beta} \pm j2\pi/l$ $(j = 1, 2, \ldots)$ are also roots of Eq. (47). However, insertion of them into Eq. (48) does not change the free vibration wave.

5. Application to railway tracks

In this section, the approach presented above is applied to the study of railway track dynamics. Ref. [10] calculated the dispersion curves up to 6000 Hz for a *free* UIC60 rail using a 2.5D FEM with 149 nodes (447 degrees of freedom) and 124 finite elements. However, for a conventional track and for frequencies up to 3000 Hz, the rail can be modelled as a single or multiple Timoshenko beams with much fewer degrees of freedom, as shown in Refs. [6–8]. It is shown below that the single- or multiple-beam models can also be described by Eq. (2), and therefore the approach of this paper is totally applicable. A set of typical parameters for the track structure are listed in Table 1. They, and those for lateral dynamics listed in Table 2, are from Refs. [6–8], with the shear modulus being slightly adjusted. These parameters are for half the structure (i.e. a single rail on half sleepers) and correspond to a track with concrete sleepers and moderately stiff rail

Table 1
Parameters for the vertical dynamics of a track

Density of the rail	$\rho = 7850\,\mathrm{kg/m^3}$
Young's modulus of the rail	$E = 2.1 \times 10^{11}\,\mathrm{N/m^2}$
Shear modulus of the rail	$G = 0.81 \times 10^{11}\,\mathrm{N/m^2}$
Loss factor of the rail	$\eta_R = 0.01$
Cross-sectional area of the rail	$A = 7.69 \times 10^{-3}\,\mathrm{m^2}$
Second moment of area of the rail cross-section	$I = 30.55 \times 10^{-6}\,\mathrm{m^4}$
Shear coefficient of the rail cross-section	$\kappa = 0.4$
Vertical rail pad stiffness	$k_{Pv} = 3.5 \times 10^8\,\mathrm{N/m}$
Rail pad loss factor	$\eta_P = 0.25$
Mass of sleeper	$m_S = 162\,\mathrm{kg}$
Sleeper spacing	$l = 0.6\,\mathrm{m}$
Vertical ballast stiffness	$k_{Bv} = 50 \times 10^6\,\mathrm{N/m}$
Loss factor of ballast	$\eta_B = 1.0$

Table 2
Parameters for the lateral dynamics of a track

Height of the rail head	$h_h = 0.039\,\mathrm{m}$
Width of the rail head	$b_h = 0.073\,\mathrm{m}$
Cross-sectional area of the rail head	$A_h = 2.847 \times 10^{-3}\,\mathrm{m}^2$
Shear coefficient of the rail head	$\kappa_h = 0.85$
Second moment of area of the rail head	$I_h = 1.264 \times 10^{-6}\,\mathrm{m}^4$
Polar second moment of area of the rail head	$I_{hp} = 1.625 \times 10^{-6}\,\mathrm{m}^4$
Equivalent polar second moment of area of the rail head	$J_h = 0.9549 \times 10^{-6}\,\mathrm{m}^4$
Height of the rail foot	$h_f = 0.0175\,\mathrm{m}$
Width of the rail foot	$b_f = 0.15\,\mathrm{m}$
Cross-sectional area of the rail foot	$A_f = 2.625 \times 10^{-3}\,\mathrm{m}^2$
Shear coefficient of the rail foot	$\kappa_f = 0.85$
Second moment of area of the rail foot	$I_f = 4.921 \times 10^{-6}\,\mathrm{m}^4$
Polar second moment of area of the rail foot	$I_{fp} = 4.988 \times 10^{-6}\,\mathrm{m}^4$
Equivalent polar second moment of area of the rail foot	$J_f = 0.2471 \times 10^{-6}\,\mathrm{m}^4$
Height of the rail web	$h_w = 0.114\,\mathrm{m}$
Width of the rail web	$b_w = 0.019\,\mathrm{m}$
Cross-sectional area of the rail web	$A_w = 2.166 \times 10^{-3}\,\mathrm{m}^2$
Second moment of area of the rail web	$I_w = 0.5716 \times 10^{-6}\,\mathrm{m}^4$
Lateral railpad stiffness	$k_{Pl} = 49.98 \times 10^6\,\mathrm{N/m}$
Lateral ballast stiffness	$k_{Bl} = 79.98 \times 10^6\,\mathrm{N/m}$

pads. Damping is introduced for the track via complex stiffness with the imaginary part being the stiffness times a loss factor.

5.1. Vertical dynamics using Timoshenko beam model

For the vertical dynamics of a railway track up to 3000 Hz, the Timoshenko beam model can be employed to model the rail. According to the Timoshenko beam theory, the differential equation for the rail subject to a unit vertical moving harmonic load is given by

$$\rho A\frac{\partial^2 w}{\partial t^2} - \kappa AG\frac{\partial^2 w}{\partial x^2} + \kappa AG\frac{\partial \psi}{\partial x} = \delta(x - x_0 - ct)\mathrm{e}^{\mathrm{i}\Omega t} + \sum_{j=-\infty}^{\infty} F_j(t)\delta(x - jl), \tag{50}$$

$$\rho I\frac{\partial^2 \psi}{\partial t^2} - EI\frac{\partial^2 \psi}{\partial x^2} - \kappa AG\frac{\partial w}{\partial x} + \kappa AG\psi = \sum_{j=-\infty}^{\infty} M_j(t)\delta(x - jl), \tag{51}$$

where w is the vertical displacement of the rail and ψ is the rotation angle of the cross-section due to the bending moment only. $F_j(t)$ is the vertical supporting force produced by the jth support and $M_j(t)$ is the torque produced by the jth support in the vertical plane. The longitudinal shear force between the rail and sleeper is neglected. Comparison has been made between situations with and without $M_j(t)$, and it is found that the difference is negligible. The reason is that even at 3000 Hz, the wavelength in the rail modelled as a Timoshenko beam is about 0.62 m, much longer than the

width (0.25 m) of a sleeper. Comparing Eqs. (50) and (51) with Eq. (8), it follows that

$$[\mathbf{M}] = \begin{bmatrix} \rho A & 0 \\ 0 & \rho I \end{bmatrix}, \quad [\mathbf{K}]_0 = \begin{bmatrix} 0 & 0 \\ 0 & \kappa AG \end{bmatrix}, \quad [\mathbf{K}]_1 = \begin{bmatrix} 0 & \kappa AG \\ -\kappa AG & 0 \end{bmatrix},$$
$$[\mathbf{K}]_2 = \begin{bmatrix} \kappa AG & 0 \\ 0 & EI \end{bmatrix}, \quad \{P_0\} = \begin{Bmatrix} 1 \\ 0 \end{Bmatrix}, \quad [\mathbf{T}]_p = \begin{bmatrix} 1 & 0 \\ 0 & 1 \end{bmatrix}, \quad \text{and} \quad \{q\} = \begin{Bmatrix} w \\ \psi \end{Bmatrix}.$$

The receptance matrix of the support including a railpad, a sleeper and the ballast, is given by

$$[\mathbf{H}(\omega)] = \begin{bmatrix} \dfrac{k_{Bv} + k_{Pv} - m_S\omega^2}{k_{Pv}[k_{Bv} - m_S\omega^2]} & 0 \\ 0 & \dfrac{12}{b_S^2 k_{Pv}} \end{bmatrix}, \tag{52}$$

where k_{Pv} and k_{Bv} are complex stiffness of the railpad and ballast, m_S is the sleeper mass, and $b_S = 0.25$ m is the width of the sleeper. The rotation of the sleeper is neglected.

As has been identified, when the load is moving the amplitude (which is the displacement divided by the load) of the displacement of the loading point is not, due to the discrete supports, constant but instead a periodic function of time. The variation of the displacement amplitude of the loading point with time t varying over $[0, l/c]$ is equivalent to the variation due to the initial loading position, x_0, varying over $[0, l]$ at $t = 0$. Figs. 1–3 show the amplitude/frequency relation

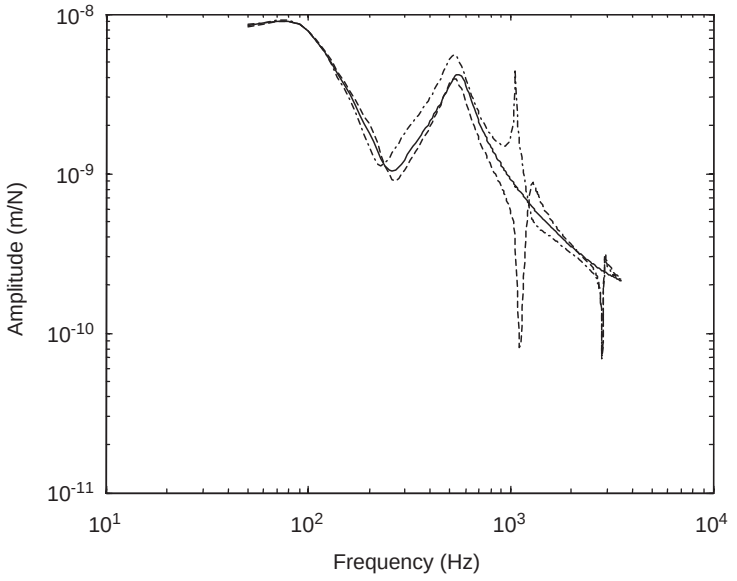

Fig. 1. Vertical displacement amplitude at the loading point for stationary load. ——, continuous support model; – – –, above sleeper; – · –, at the mid-span.

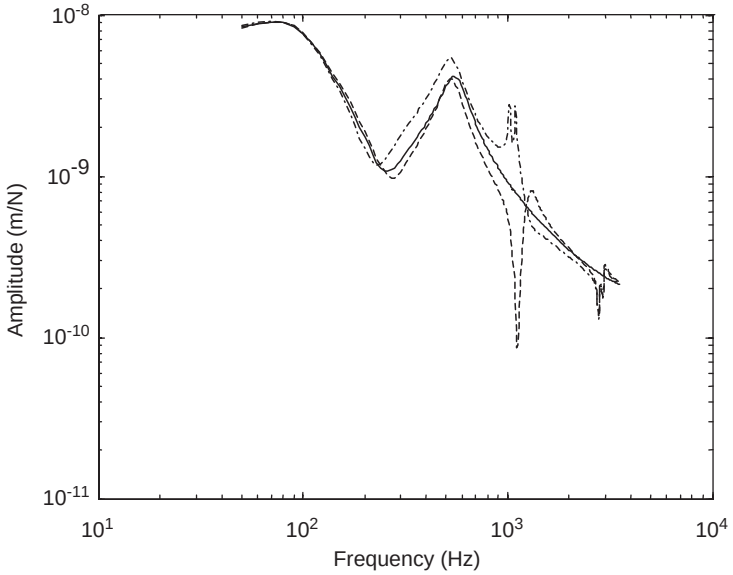

Fig. 2. Vertical displacement amplitude at the loading point for load speed = 40 m/s. ——, continuous support model; – – –, above sleeper; – · –, at the mid-span.

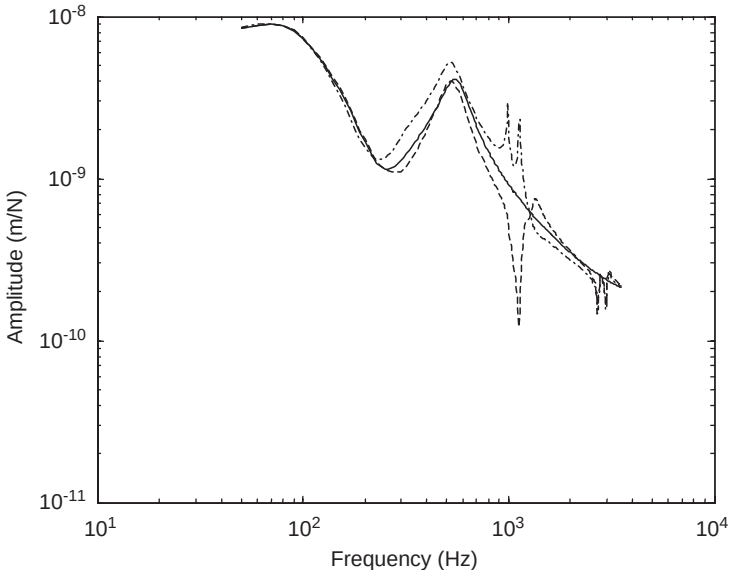

Fig. 3. Vertical displacement amplitude at the loading point for load speed = 80 m/s. ——, continuous support model; – – –, above sleeper; – · –, at the mid-span.

at $t = 0$ of the loading point for two initial loading positions (at mid-span and above a sleeper) and three load speeds (0, 40 and 80 m/s). Also shown is the results produced from the continuous support model (Eq. (46)). From these figures, it can be seen that:

(1) The effect of the load speed on the response of the continuous support model is negligible for the whole frequency range considered. However, for the discrete support model the load speed does have an effect near the pinned–pinned frequency (about 1000 Hz). The resonance and anti-resonance at the pinned–pinned frequency for a stationary load has been revealed not only by calculation as in Fig. 1, but also by measurement [11]. At mid-span, the load speed splits the peak at the pinned–pinned frequency into two peaks. The heights of the two peaks decrease and the frequency spacing between them increases as the load speed increases. On the other hand, for the response above a sleeper, the depth of the dip at the pinned–pinned frequency is reduced by the load speed.

(2) For frequencies less than 200 Hz (termed here the *low-frequency range*), the continuous support model gives almost the same results as the discrete support model, irrespective of the load speed and loading position. In other words, the continuous support model for the vertical track dynamics is appropriate for this frequency range, apart from a small modulation of the track stiffness at the sleeper passing frequency. This finding confirms the track model used in ground vibration modelling [12,13] in which the considered frequencies are less than 200 Hz and the track is described using the continuous support model.

(3) For higher frequencies, the dependence is clearly shown in these figures of the amplitude on the loading position. In other words, for a given load frequency, the displacement amplitude of the loading point fluctuates about an average value when the load moves within a sleeper bay. As identified above, the frequency of the fluctuation is the sleeper-passing frequency which is 116 Hz at 250 km/h (69.4 m/s). The fluctuation is obvious (can be 50% of the average) for frequencies from 200 to 800 Hz (the *middle-frequency range*) and huge for those close to the pinned–pinned frequency (frequencies higher than 800 Hz are termed the *high-frequency range*). Compared to load frequencies within the *high-frequency range*, the sleeper-passing frequency is small (less than $\frac{1}{8}$) for possible train speeds. However, due to its huge fluctuation at the pinned–pinned frequency, the amplitude within a period of variation of the load may still vary significantly. In the *middle-frequency range*, the sleeper-passing frequency can be as high as half the load frequency and therefore the amplitude within a period of variation of the load cannot be approximated as a constant.

(4) The above observations indicate that, for vehicle/track interaction problems in which only the vertical dynamics of the track needs to be considered, only in the *low-frequency range* can the vehicles be regarded as stationary and are excited by a roughness strip passing between wheel and rail at the train speed. In this frequency range, the continuous support track model can be used. In the *middle- and high-frequency ranges*, improvements are desired to such a modelling approach. Of course, for rolling noise problems, such a modelling approach would not introduce significant errors if noise levels in dB are presented for $\frac{1}{3}$ octave bands, as confirmed by measurements [14]. However, the load speed is important for short-pitch corrugation growth since the pinned–pinned vibration plays a vital role in corrugation development [15].

5.2. Lateral dynamics using the multiple beam model

In Ref. [7], a multiple-beam model is proposed for the lateral vibration of a rail. In this model the rail is divided into three parts each with a rectangular cross-section: the head (indicated by subscript h) and the foot (indicated by subscript f) are represented by two infinite Timoshenko

beams which can be subjected to both bending and torsion and the web (indicated by subscript w) is replaced by an array of vertical beams along the rail which connect the head and foot. The effects of the web twisting and bending in the rail direction are neglected. The geometric properties of a rectangle are described by h, the height, b, the width, A, the cross-sectional area, I, the second moment of area, J, the equivalent polar second moment of area, I_p, the polar second moment of area and κ, the shear coefficient. The geometric parameters for lateral vibration can be evaluated from the height h and width b of a rectangle. The geometric parameters are listed in Table 2.

At the top of the head, a unit moving (at speed c) lateral harmonic load of frequency Ω is applied. The lateral displacement of a beam is denoted by υ, the rotation angle of its cross-section due to the bending moment only by ψ and the torsion angle of the beam by θ. The differential equation of the track is derived in Appendix A and given by

$$[\mathbf{M}]\frac{\partial^2}{\partial t^2}\{q(x,t)\}+[\mathbf{K}]_0\{q(x,t)\}+[\mathbf{K}]_1\frac{\partial}{\partial x}\{q(x,t)\}-[\mathbf{K}]_2\frac{\partial^2}{\partial x^2}\{q(x,t)\}$$
$$=\begin{Bmatrix}\delta(x-x_0-ct)\mathrm{e}^{\mathrm{i}\Omega t}\\ 0\\ \frac{h_h}{2}\delta(x-x_0-ct)\mathrm{e}^{\mathrm{i}\Omega t}\\ \sum_{j=-\infty}^{\infty}V_j(t)\delta(x-jl)\\ \sum_{j=-\infty}^{\infty}T_j(t)\delta(x-jl)\\ \sum_{j=-\infty}^{\infty}\left(M_j(t)-\frac{h_f}{2}V_j(t)\right)\delta(x-jl)\end{Bmatrix}, \tag{53}$$

where

$$\{q(x,t)\}=(\upsilon_h,\psi_h,\theta_h,\upsilon_f,\psi_f,\theta_f)^{\mathrm{T}}, \tag{54}$$

$V_j(t)$, $T_j(t)$ and $M_j(t)$ are the lateral force, bending torque and torsion torque exerted on the rail foot by the jth support.

Comparison of this with Eq. (8) indicates that

$$\{P_0\}=\left(1,0,\frac{h_h}{2},0,0,0\right)^{\mathrm{T}}, \tag{55}$$

$$\{F_j(t)\}=\left(V_j(t),T_j(t),M_j(t)-\frac{h_f}{2}V_j(t)\right)^{\mathrm{T}}. \tag{56}$$

The matrix $[\mathbf{T}]_p$ in Eq. (9) is of order 6×3 and only three elements, $T_p(4,1)$, $T_p(5,2)$ and $T_p(6,3)$ are non-zero but instead, $T_p(4,1)=T_p(5,2)=T_p(6,3)=1$.

The receptance matrix of the support in accordance with the supporting force vector defined in Eq. (56) is of order 3×3, and is given by

$$[\mathbf{H}(\omega)] = \begin{bmatrix} \dfrac{k_{Pl} + k_{Bl} - m_s\omega^2}{k_{Pl}(k_{Bl} - m_s\omega^2)} + \dfrac{3h_f^2}{b_f^2 k_{Pv}} & 0 & \dfrac{6h_f}{b_f^2 k_{Pv}} \\ 0 & \dfrac{12}{b_S^2 k_{Pl}} & 0 \\ \dfrac{6h_f}{b_f^2 k_{Pv}} & 0 & \dfrac{12}{b_f^2 k_{Pv}} \end{bmatrix}. \tag{57}$$

To derive this receptance matrix it has been assumed that the sleeper vibrates only in the lateral direction.

Figs. 4–6 present the lateral displacement amplitude of the loading point at $t = 0$ for two initial loading positions (at mid-span and above a sleeper) and three load speeds (0, 40 and 80 m/s), as well as the results from the continuous support model (Eq. (46)). For the case of a stationary load (Fig. 4), discussions have been given in Ref. [8]. As for the track vertical dynamics, the results here show a significant effect of the load speed on the pinned–pinned vibration which occurs at about 500 Hz: in addition to splitting the peak into two, the load speed greatly reduces the peak and dip at this frequency. For frequencies below 250 Hz, the response at mid-span and that above a sleeper are close to each other, implying that in this frequency range, the amplitude of the loading point can be regarded as a constant as the load passes a sleeper bay. Near the pinned-pinned frequency however, the amplitude at the loading point changes significantly as the load passes a

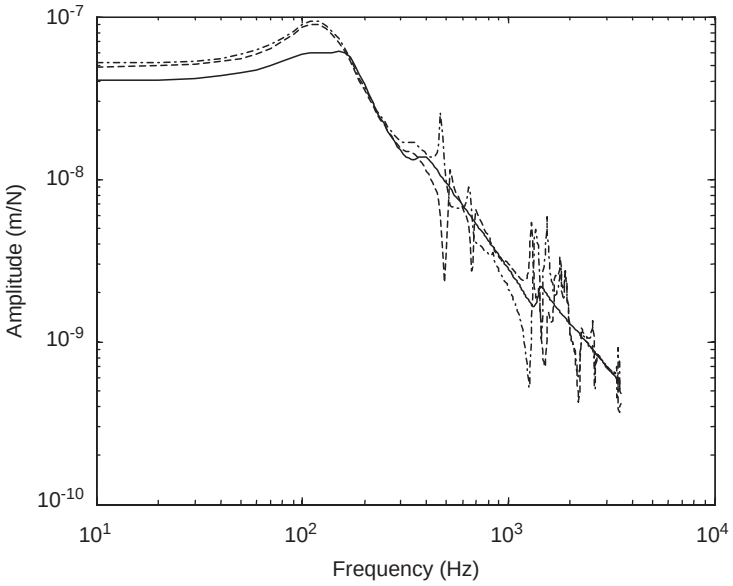

Fig. 4. Lateral displacement amplitude at the loading point for stationary load. ——, continuous support model; – – –, above sleeper; – · –, at the mid-span.

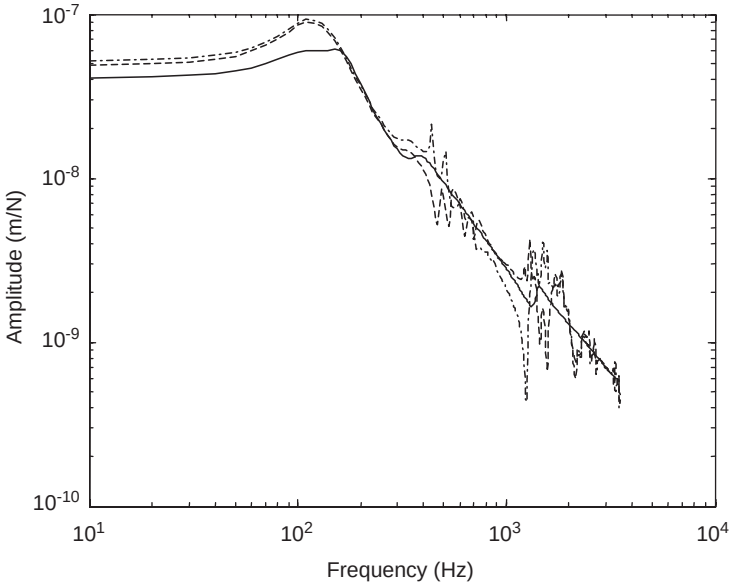

Fig. 5. Lateral displacement amplitude at the loading point for load speed = 40 m/s. ——, continuous support model; – – –, above sleeper; – · –, at the mid-span.

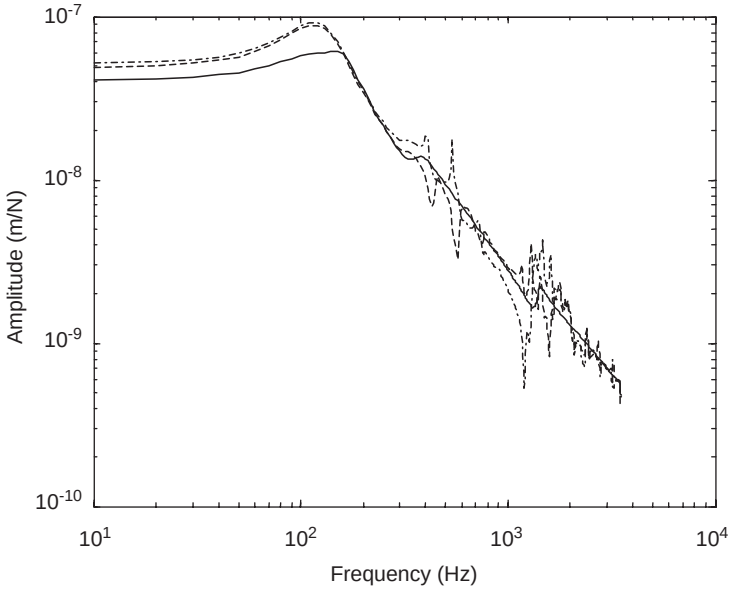

Fig. 6. Lateral displacement amplitude at the loading point for load speed = 80 m/s. ——, continuous support model; – – –, above sleeper; – · –, at the mid-span.

sleeper bay. If the load speed is very high (e.g. 83 m/s that is 300 km/h), the sleeper passing frequency (139 Hz) is not very small compared with the pinned-pinned frequency. In this case, the amplitude of the loading point changes significantly within one cycle of excitation.

A remarkable observation from these figures is that for frequencies below about 200 Hz, the results from the continuous support model are much lower than those from the discrete support model. This observation can also be made by comparing Fig. 7 in Ref. [6] and Fig. 1 in Ref. [7] for the case of stationary load. In other words, the continuous support model is inappropriate for lateral track vibration, even for low frequencies.

6. Conclusion

In this paper, a general, wavenumber-based, approach is proposed for the computation of the response of periodically supported structures subject to a moving or stationary harmonic load. The structures can be described using either a multiple-beam model or a two-and-half-dimensional finite element model if the beam model is inappropriate. The supports may have arbitrary degrees of freedom, either translational or rotational. Equations for free vibration propagation constants, which have been previously derived for simple periodic structures, are yielded straightforwardly from this approach.

The amplitude (displacement divided by load) of the displacement of a periodic structure subject to a moving harmonic load is not constant but, if observed from the moving load, a periodic function of time t with the period equal to the bay-passing time. The Fourier coefficients of this periodic function are expressed explicitly in terms of an integral over the wavenumber in the longitudinal direction.

An equivalent continuous support model is introduced by evenly distributing the receptance of the supports along each bay. Observed from the moving load, the amplitude of the displacement is constant, i.e., the displacement of the continuous support model is purely time-harmonic.

Results are produced for a conventional ballasted track subject to a harmonic load of different frequencies moving at different load speeds. From these results the effects of the load speed and the modelling of the supports have been identified.

The load speed has a significant effect on the pinned–pinned vibration of the track. The height (depth) of the peak (dip) at the pinned–pinned frequency decreases as the load speed increases. Since the pinned–pinned vibration plays a vital role in the development of short-pitch rail corrugations, the motion of wheels, which has in general been neglected in previous studies, must be included in the research into short-pitch rail corrugations and roughness growth.

For the vertical dynamics of the track and for load frequencies less than 200 Hz, the fluctuation of the displacement amplitude of the discrete support model as the load passes a sleeper bay is negligible. The displacement amplitude is almost identical to that from the continuous support model and is almost independent of the load speed if it is within the range of possible train speeds. This confirms the usefulness of the continuous support model in the study of train-induced ground vibration. For load frequencies higher than 200 Hz the displacement amplitude observed from the moving load may change significantly within a period of variation of the load.

For load frequencies less than 250 Hz in the lateral dynamics of the track, the fluctuation of the displacement amplitude of the discrete support model as the load passes a sleeper bay is also

negligible. However, for the lateral dynamics of the track, the continuous support model is totally inappropriate.

Acknowledgement

This work is supported by the EPSRC and RRUK under project A3: Railway noise: curve squeal, roughness growth, friction and wear.

Appendix A

This appendix is given for the derivation of the differential equation of motion for the lateral dynamics of a track. The lateral displacement of a beam is denoted by υ, the rotation angle of its cross-section due to the bending moment only by ψ and the torsion angle of the beam by θ. The bending moment and shear force per unit length of rail at the top end of the web are denoted by M_h and Q_h. Those at the bottom are denoted by M_f and Q_f. At the top of the head, a unit moving (at speed c) lateral harmonic load of frequency Ω is applied (Fig. A.1).

The differential equations of motion for the head are given by

$$\rho A_h \frac{\partial^2 \upsilon_h}{\partial t^2} - \kappa_h A_h G \frac{\partial^2 \upsilon_h}{\partial x^2} + \kappa_h A_h G \frac{\partial \psi_h}{\partial x} = \delta(x - x_0 - ct)\mathrm{e}^{\mathrm{i}\Omega t} - Q_h, \tag{A.1a}$$

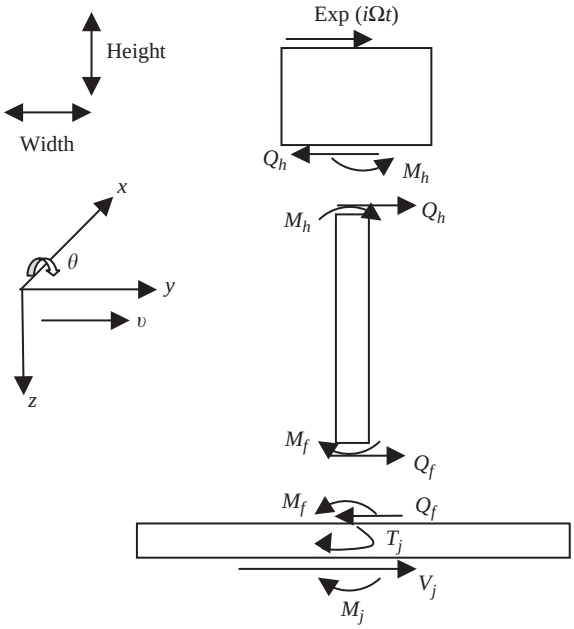

Fig. A.1. Forces on the rail.

$$\rho I_h \frac{\partial^2 \psi_h}{\partial t^2} - EI_h \frac{\partial^2 \psi_h}{\partial x^2} - \kappa_h A_h G \frac{\partial \upsilon_h}{\partial x} + \kappa_h A_h G \psi_h = 0, \tag{A.1b}$$

$$\rho I_{hp} \frac{\partial^2 \theta_h}{\partial t^2} - GJ_h \frac{\partial^2 \theta_h}{\partial x^2} = -M_h + Q_h \frac{h_h}{2} + \frac{h_h}{2} \delta(x - x_0 - ct) e^{i\Omega t}. \tag{A.1c}$$

If denoting

$$\{q(x,t)\} = (\upsilon_h, \psi_h, \theta_h, \upsilon_f, \psi_f, \theta_f)^{\mathrm{T}} \tag{A.2}$$

then Eq. (A.1) can be written as

$$[\mathbf{M}]_h \frac{\partial^2}{\partial t^2}\{q(x,t)\} + [\mathbf{K}]_{0h}\{q(x,t)\} + [\mathbf{K}]_{1h} \frac{\partial}{\partial x}\{q(x,t)\} - [\mathbf{K}]_{2h} \frac{\partial^2}{\partial x^2}\{q(x,t)\} = \begin{Bmatrix} \delta(x - x_0 - ct) e^{i\Omega t} - Q_h \\ 0 \\ \frac{h_h}{2} \delta(x - x_0 - ct) e^{i\Omega t} - M_h + \frac{h_h}{2} Q_h \\ 0 \\ 0 \\ 0 \end{Bmatrix}, \tag{A.3}$$

where $[\mathbf{M}]_h$, etc. are 6×6 matrices.

Similarly for the foot,

$$\rho A_f \frac{\partial^2 \upsilon_f}{\partial t^2} - \kappa_f A_f G \frac{\partial^2 \upsilon_f}{\partial x^2} + \kappa_f A_f G \frac{\partial \psi_f}{\partial x} = \sum_{j=-\infty}^{\infty} V_j(t) \delta(x - jl) - Q_f, \tag{A.4a}$$

$$\rho I_f \frac{\partial^2 \psi_f}{\partial t^2} - EI_f \frac{\partial^2 \psi_f}{\partial x^2} - \kappa_f A_f G \frac{\partial \upsilon_f}{\partial x} + \kappa_f A_f G \psi_f = \sum_{j=-\infty}^{\infty} T_j(t) \delta(x - jl), \tag{A.4b}$$

$$\rho I_{fp} \frac{\partial^2 \theta_f}{\partial t^2} - GJ_f \frac{\partial^2 \theta_f}{\partial x^2} = -M_f - Q_f \frac{h_f}{2} + \sum_{j=-\infty}^{\infty} \left(M_j(t) - \frac{h_f}{2} V_j(t) \right) \delta(x - jl), \tag{A.4c}$$

where $V_j(t)$, $T_j(t)$ and $M_j(t)$ are the lateral force, bending and torsional torques exerted on the rail foot by the jth support. These equations are also written in the compact form

$$[\mathbf{M}]_f \frac{\partial^2}{\partial t^2}\{q(x,t)\} + [\mathbf{K}]_{0f}\{q(x,t)\} + [\mathbf{K}]_{1f}\frac{\partial}{\partial x}\{q(x,t)\} - [\mathbf{K}]_{2f}\frac{\partial^2}{\partial x^2}\{q(x,t)\}$$
$$= \begin{Bmatrix} 0 \\ 0 \\ 0 \\ \sum_{j=-\infty}^{\infty} V_j(t)\delta(x-jl) - Q_f \\ \sum_{j=-\infty}^{\infty} T_j(t)\delta(x-jl) \\ -M_f - \frac{h_f}{2}Q_f + \sum_{j=-\infty}^{\infty}\left(M_j(t) - \frac{h_f}{2}V_j(t)\right)\delta(x-jl) \end{Bmatrix}. \tag{A.5}$$

The differential equations of motion for the web are given by those for a single beam element (without axial deformation):

$$[\mathbf{m}]_w \begin{Bmatrix} \frac{\partial^2 \upsilon_h}{\partial t^2} - \frac{h_h}{2}\frac{\partial^2 \theta_h}{\partial t^2} \\ \frac{\partial^2 \theta_h}{\partial t^2} \\ \frac{\partial^2 \upsilon_f}{\partial t^2} + \frac{h_f}{2}\frac{\partial^2 \theta_f}{\partial t^2} \\ \frac{\partial^2 \theta_f}{\partial t^2} \end{Bmatrix} + [\mathbf{k}]_w \begin{Bmatrix} \upsilon_h - \frac{h_h}{2}\theta_h \\ \theta_h \\ \upsilon_f + \frac{h_f}{2}\theta_f \\ \theta_f \end{Bmatrix} = \begin{Bmatrix} Q_h \\ M_h \\ Q_f \\ M_f \end{Bmatrix}, \tag{A.6}$$

where

$$[\mathbf{m}]_w = \frac{\rho b_w h_w}{420}\begin{bmatrix} 156 & -22h_w & 54 & 13h_w \\ -22h_w & 4h_w^2 & -13h_w & -3h_w^2 \\ 54 & -13h_w & 156 & 22h_w \\ 13h_w & -3h_w^2 & 22h_w & 4h_w^2 \end{bmatrix}, \tag{A.7}$$

$$[\mathbf{k}]_w = \frac{EI_w}{h_w^3}\begin{bmatrix} 12 & -6h_w & -12 & -6h_w \\ -6h_w & 4h_w^2 & 6h_w & 2h_w^2 \\ -12 & 6h_w & 12 & 6h_w \\ -6h_w & 2h_w^2 & 6h_w & 4h_w^2 \end{bmatrix} \tag{A.8}$$

are the mass and stiffness matrices. Eq. (A.6) can be rewritten as

$$[\mathbf{M}]_w \frac{\partial^2}{\partial t^2}\{q(x,t)\} + [\mathbf{K}]_{0w}\{q(x,t)\} = \begin{Bmatrix} Q_h \\ 0 \\ M_h - \dfrac{h_h}{2} Q_h \\ Q_f \\ 0 \\ M_f + \dfrac{h_f}{2} Q_f \end{Bmatrix}, \tag{A.9}$$

where

$$[\mathbf{M}]_w = [\mathbf{R}]^{\mathrm{T}}[\mathbf{m}]_w[\mathbf{R}], \tag{A.10}$$

$$[\mathbf{K}]_{0w} = [\mathbf{R}]^{\mathrm{T}}[\mathbf{k}]_w[\mathbf{R}], \tag{A.11}$$

$$[\mathbf{R}] = \begin{bmatrix} 1 & 0 & -\dfrac{h_h}{2} & 0 & 0 & 0 \\ 0 & 0 & 1 & 0 & 0 & 0 \\ 0 & 0 & 0 & 1 & 0 & \dfrac{h_f}{2} \\ 0 & 0 & 0 & 0 & 0 & 1 \end{bmatrix}. \tag{A.12}$$

Addition of Eqs. (A.3), (A.5) and (A.9) gives the differential equation of the track for lateral dynamics, i.e. Eq. (53) in which

$$[\mathbf{M}] = [\mathbf{M}]_h + [\mathbf{M}]_f + [\mathbf{M}]_w \tag{A.13}$$

and similar for $[\mathbf{K}]_0$, $[\mathbf{K}]_1$ and $[\mathbf{K}]_2$.

References

[1] D.J. Mead, Wave propagation in continuous periodic structures: research contributions from Southampton, *Journal of Sound and Vibration* 190 (3) (1996) 495–524.
[2] P.J. Remington, Wheel/rail rolling noise—Part I: theoretical analysis, *Journal of the Acoustical Society of America* 81 (1987) 1805–1823.
[3] S. Müller, A linear wheel–track model to predict instability and short pitch corrugation, *Journal of Sound and Vibration* 227 (5) (1999) 899–913.
[4] P.M. Belotserkovskiy, On the oscillations of infinite periodic beams subject to a moving concentrated force, *Journal of Sound and Vibration* 193 (3) (1996) 705–712.
[5] A. Nordborg, Wheel/rail noise generation due to nonlinear effects and parametric excitation, *Journal of the Acoustical Society of America* 111 (4) (2002) 1772–1781.
[6] T.X. Wu, D.J. Thompson, A double Timoshenko beam model for vertical vibration analysis of railway track at high frequencies, *Journal of Sound and Vibration* 224 (2) (1999) 329–348.
[7] T.X. Wu, D.J. Thompson, Analysis of lateral vibration behaviour of railway track at high frequencies using a continuously supported multiple beam model, *Journal of the Acoustical Society of America* 106 (3) (1999) 1369–1376.

[8] T.X. Wu, D.J. Thompson, Application of a multiple-beam model for lateral vibration analysis of a discretely supported rail at high frequencies, *Journal of the Acoustical Society of America* 108 (3) (2000) 1341–1344.
[9] X. Sheng, C.J.C. Jones, D.J. Thompson, Modelling ground vibration from rail traffic using discrete wavenumber finite and boundary element methods, University of Southampton, Institute of Sound and Vibration Research, Technical Memorandum 899, 2002.
[10] L. Gavrić, Computation of propagative waves in free rail using a finite element technique, *Journal of Sound and Vibration* 185 (3) (1995) 531–543.
[11] S.L. Grassie, R. Gregory, D. Harrison, K. Johnson, The dynamic response of railway track to high frequency vertical excitation, *Journal of Mechanical Engineering Science* 24 (2) (1982) 77–90.
[12] X. Sheng, C.J.C. Jones, D.J. Thompson, A theoretical study on the influence of the track on train-induced ground vibration, *Journal of Sound and Vibration* 272 (3–5) (2004) 909–936.
[13] X. Sheng, C.J.C. Jones, D.J. Thompson, A theoretical model for ground vibration from trains generated by vertical track irregularities, *Journal of Sound and Vibration* 272 (3–5) (2004) 937–965.
[14] D.J. Thompson, B. Hemsworth, N. Vincent, Experimental validation of the TWINS prediction program for rolling noise—Part II: Results, *Journal of Sound and Vibration* 193 (1996) 137–147.
[15] S.L. Grassie, Rail corrugation: advances in measurement, understanding and treatment, *Proceedings of the Sixth International Conference on Contact Mechanics and Wear of Rail/Wheel Systems*, 2003, 11–19pp.